Fisheries Research 107 (2011) 147–158

Contents lists available at ScienceDirect

Fisheries Research

journal homepage: www.elsevier.com/locate/fishres

Field demonstration of a novel towed, area bubble-plume zooplankton (*Calanus sp.*) harvester

Eduardo Grimaldo[a,*], Ira Leifer[b], Svein Helge Gjøsund[a], Roger B. Larsen[c], Henrik Jeuthe[c], Sünnje Basedow[c]

[a] SINTEF Fisheries and Aquaculture, SINTEF SeaLab, Brattorkaia 17, NO-7465 Trondheim, Norway
[b] Marine Sciences Institute, University of California, Santa Barbara, CA 93106, USA
[c] University of Tromsø, Breivika NO-9037 Tromsø, Norway

ARTICLE INFO

Article history:
Received 19 June 2010
Received in revised form 20 October 2010
Accepted 20 October 2010

Keywords:
Harvesting zooplankton
Calanus
Air bubbles
Bubble plume
Engineered upwelling
Upwelling velocity

ABSTRACT

This paper presents the field testing of a new technology to harvest marine copepods (*Calanus sp.*) by bubble-induced upwelling. Two large-scale bubble rafts, a 21 m^2 and a flexible 75 m^2 bubble raft with tow-parallel and tow-perpendicular sparger elements, respectively, were tested in the sea with high *Calanus* densities in the upper 25 m. Bubble-driven upwelling velocities (V_{up}) measured with different air flows (Q) and source depths (z_0), gave $V_{up} \sim Q^{0.27}$ with stratified water, and were in agreement with other results for stratified conditions. Bubble trawls significantly enhanced *Calanus* concentrations in the upper water column: up to 1416%, with the best results for the transverse sparger raft, which also was tested with weak stratification. Bubble trawl performance also was affected by the stratification, with the highest enhancement for the lowest stratification. Catch species analysis showed reduced bycatch. Thus, this new harvesting technology showed a potential to develop an economically robust, environmentally benign, and sustainable fishery on a renewable resource at lower trophic levels in the food web, within the context of ecosystem-based management.

1. Introduction

1.1. Overview

In recent years there has been increased interest in the exploitation of marine zooplankton such as copepods and krill. This has been motivated by the increasing demand for marine bio-resources for human consumption in general, and in particular the growing demand for feed in aquaculture. In Nordic Seas, zooplankton are a key component in the energy transfer from primary producers to higher trophic levels such as herring, capelin, salmon, cod larvae and juveniles, and other species (Skjoldal, 2005). Roughly 70–80% of the zooplankton production in these waters is made up by copepods of the genus *Calanus* (Tande and Miller, 2000). According to general ecological theory about 10% of this production is available to the next trophic level (Lalli and Parsons, 1997). The total annual production of *Calanus sp.* is estimated at 75 million tons y^{-1} for the Nordic Seas (Aksnes and Blindheim, 1996) and 300 million tons (mainly *C. finmarchicus*) y^{-1} for the Norwegian Sea only (Skjoldal et al., 2004). This vast resource has great economic potential because it is rich in marine lipids, proteins, amino acids, and pigments. Further, by nature of being low on the food chain it has far lower bioaccumulation of heavy metals, organo-chlorides, dioxins, and other pollutants than higher trophic species (Mizukawaa et al., 2009). Therefore, copepod fisheries have the potential to support the growth of new ventures in markets for functional food, food ingredients, and nutrition products. However, development of a copepod fishery must be pursued wisely (Nicol and Endo, 1999) using the best technology at hand, and implemented within a solid ecosystem based management regime, particularly given the importance of copepods to the marine ecosystem.

In open Norwegian waters, *Calanus spp.* widely are found in the upper 50 m during the productive period from April to August (Falkenhaug et al., 1997; Dahle and Kaartvedt, 2000). For practical reasons, harvesting concentrates on adults (CVI) and the life stages CIV and CV (the two last copepodite stages before becoming adults), because in these stages copepods have achieved sufficient body mass–body lengths are from 2.3 to 5.0 mm, depending upon species (Unstad and Tande, 1991). In addition, copepod lipid content increases with increasing stage, with the two oldest stages being the most lipid rich (Kattner and Krause, 1987).

Currently, *Calanus* harvesting uses fine-meshed trawls (~500 μm bar length) with mouth openings that range from 40 to 100 m^2, depending on the vessel size (Snorre Angell, Calanus

* Corresponding author. Tel.: +47 40624014; fax: +47 93270701.
E-mail address: Eduardo.Grimaldo@sintef.no (E. Grimaldo).

0165-7836/$ – see front matter © 2010 Elsevier B.V. All rights reserved.
doi:10.1016/j.fishres.2010.10.018

Nomenclature

Q (L min^{-1})	air flow (corrected to STP)
Q_A (L min^{-1})	air flow per square meter (corrected to STP)
Q^b (L min^{-1})	power law
H_s (m)	wave significant height
r (μm)	bubble spherical radius
t (s)	transit time
V (cm s^{-1})	velocity
V_{up} (cm s^{-1})	vertically averaged plume upwelling velocities
V_{AG} (cm s^{-1})	bubble-copepod aggregate velocity
T (C°)	temperature
S (ppm)	salinity
ρ (mg L^{-1})	density
F (mg L^{-1})	fluorescence
z (m)	depth
z_0 (m)	dye release depth
z_T (cm)	depth of sampling net mouth centre
C_C (ml)	catch of control nets 1
C_{C2} (ml)	catch of control nets 2
C_{Cm} (ml)	mean catch of C_{C1} and C_{C2}
C_T (ml)	catch of test nets1
ε	$\varepsilon > 1$ enhancement, $\varepsilon < 1$ reduction. Defined as C_T/C_C.

AS, Sortland-Norway, Pers. Comm., 2009). However these trawls may be unsuitable for large-scale zooplankton harvesting because their very high towing resistance translates to high fuel consumption and CO_2 emissions. Moreover, several unwanted species are included in the harvested biomass. This study presents field test results of a new fisheries approach, incorporating bubble flotation into the harvest process to greatly reduce costs and negative ecological impacts.

The goal of bubble flotation-enhanced harvesting is to use bubbles to collect and transport *Calanus* vertically from a range of depths, depositing and concentrating them in a thin surface or mid-depth layer. Vertical concentration increases zooplankton harvesting efficiency by increasing the catch for a given trawl opening and resistance. In addition, bubbles are far less efficient at collecting and transporting larger species, such as fingerlings, which thus will be concentrated less or not at all in the target *Calanus* layer, i.e., the approach provides species selectivity. Also, bubbles can lift jellyfish out of the trawl path, preventing them from clogging the net.

1.2. Air bubble technology/bubble-driven upwelling/engineered bubble plumes

The two primary mechanisms underlying a bubble fishery are upwelling (Leifer et al., 2009) and attachment/flotation. As bubbles rise, they transfer momentum to the surrounding fluid, creating the upwelling flow, which transports deeper water upwards, including entrained zooplankton. For bubble attachment, small bubbles attach and add positive buoyancy to the zooplankton, lifting them upwards. Real-world applications involve both of these synergistic processes.

1.2.1. Bubble attachment

Bubbles effectively accumulate surfactants through the process termed sparging or flotation. Surfactants are surface active substances including surfactant-bacteria and particles with hydrophilic and hydrophobic sites that energetically prefer to be at air–water interfaces. This bubble collection and transport process is central to wastewater treatment microflotation (Persechini et al., 2000), mining airlift separators (Mao and Yoon, 1997), bioreactors (Wu, 1995), and marine aggregate formation (Mari, 1999). Surfactants affect bubble properties, decreasing gas exchange and rise velocity and thus decreasing dissolution (Leifer and Patro, 2002). Surfactants also stabilize bubbles against breakup (Johnson and Cooke, 1980).

Attachment requires several steps. First, the bubble trajectory must intersect the zooplankton close enough for the two to touch. Then, the bubble and zooplankton must attach, rather than "bounce." Finally, the bubble must remain attached long enough to lead to significant vertical advection. Smaller (<300 μm radius) bubbles are more likely to attach to *Calanus* because of their slower rise velocities (<6 cm s^{-1}), and because their size is comparable to key *Calanus* dimensions, such as thorax, legs, and antennae. However, because small bubble buoyancy is minimal, they provide little lift buoyancy force. Given that *Calanus* are slightly negatively buoyant; this can lead to minimal or negligible upwards motion unless several small bubbles attach to the copepod.

Laboratory studies showed that the highest zooplankton attachment was for bubbles in the range $50 < r < 300$ μm (own data, unpublished), where r is the equivalent spherical radius. Although larger bubbles have greater buoyancy, their attachment probability is lower (own data, unpublished). Bubbles comparable in size or larger than *Calanus* – circa 1000-μm radius – have well developed turbulent wakes and boundary layers, and rise fast (25–30 cm s^{-1}) compared to small bubbles (Leifer and Patro, 2002). These large bubbles tend to displace the *Calanus* along streamlines around the bubble as they pass, leading to negligible attachment probability.

After attachment, the bubble-copepod aggregate rises with a velocity, V_{AG}, determined by the drag resistance of the *Calanus*-bubble aggregate and the buoyancy force, until bubble detachment (or surfacing). In laboratory studies, a linear relationship was found between r and V_{AG}, from 2.5 to 9.0 cm s^{-1} with the highest rise velocity for a 341-μm radius bubble (own data, unpublished). Because *Calanus* are mobile, bubble detachment by body motions can be significant and reduces the *Calanus* vertical advection distance. Then, a combination of *Calanus*'s negative buoyancy and active swimming towards its original depth likely will cause sinking. Thus, successful flotation requires the attachment time scale to be sufficiently shorter than the detachment time scale. Due to detachment, flotation of more active *Calanus* is less efficient, mimicking natural selection.

1.2.2. Bubble-driven upwelling flow

For sufficiently high bubble concentration, synergistic interactions in bubble plumes create fluids with distinct properties from the surrounding fluid (Leifer et al., 2006). Bubble plumes transfer momentum to the surrounding fluid; creating an upwelling flow, see review in Leifer et al. (2009). The upwelling flow decreases bubble gas exchange with the surrounding fluid because of the reduced transit time across the water column, enhancing bubble survival against dissolution (Leifer et al., 2006). For point-source bubble plumes, larger fluid velocities are at a peak along the centerline decreasing radially with a Gaussian profile (Milgram, 1983). The fluid velocity increases with height above the source in non-stratified fluids due in part to the increase in buoyancy flux from decreasing hydrostatic pressure. At the surface, the upwelled fluid spreads out in a horizontal intrusion, the outwelling flow.

Thermal and haline stratification are common in the marine environment, with cooler and/or more saline (denser) water at greater depth. Thus, marine upwelling flows lift water with increasingly negative buoyancy. Upon encountering a steep density gradient, the bubble plume can significantly (or completely) detrain plume fluid into a horizontal intrusion; however, the bubbles continue rising, entraining new water, unlike for a continuum (single phase) plume such as a sewage outfall (McDougall, 1978). Such horizontal intrusions deposit any transported zooplankton, marine

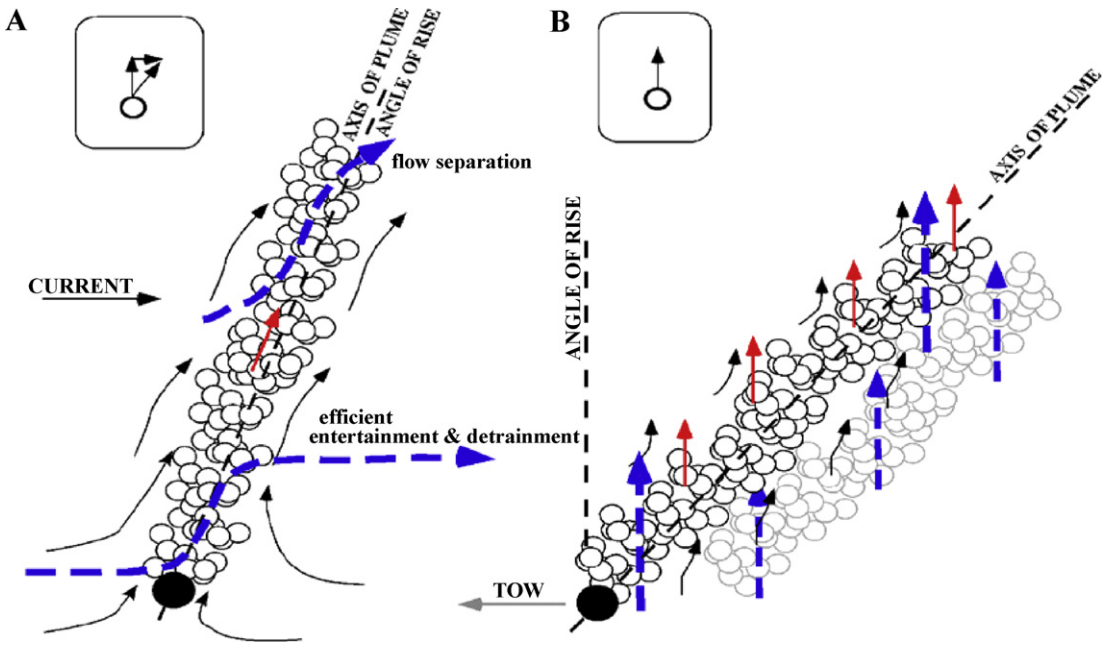

Fig. 1. Two dimensional schematic of a bubble plume for (A) a fixed bubble source in a uniform horizontal current and (B) towed bubble source through quiescent water. Inset shows details of individual bubble motions. Red and black arrows pertain to bubbles and entrained water, respectively. Grayed bubbles represent plume several seconds earlier, and remnant, persistent fluid motions. (For interpretation of the references to colour in this figure legend, the reader is referred to the web version of the article.)

particles, and dissolved gases in a layer, and have been identified in the field (Solomon et al., 2009; Leifer et al., 2009; Leifer and Judd, 2002). Sufficiently strong bubble plumes can support the upwelled fluid through the density stratification to the sea surface.

Most published field bubble plume studies are for stationary bubble plumes in static water (e.g., lake destratification studies) (Schadlow, 1992; Lemckert and Imberger, 1993; Singleton et al., 2007), natural marine hydrocarbon seeps (Leifer et al., 2000, 2009; Leifer and Boles, 2005), or gas blowouts (Topham, 1975; Milgram, 1983). However, typical fisheries applications would involve a towed bubble plume, which has not been studied before.

Potentially, there is a significant difference between a stationary (i.e., fixed) source bubble plume in a uniform horizontal current (Fig. 1A) and a towed source bubble plume through quiescent water (Fig. 1B), even though both geometries appear similar. For the former, each bubble rises and is advected by the horizontal currents. As a result, the fluid motions and bubble plume motions are aligned along the plume axis. This allows the bubbles to accelerate the fluid throughout the entire water column. In contrast, for quiescent water (Fig. 1B), bubbles rise vertically. Thus, for a towed bubble source, the apparent plume angle is vertical as are the fluid motions. However, they are not aligned with the angle of the plume. As a result, a parcel of water experiences vertical advection as a short pulse from the passing bubble sheet, rather than a sustained force. Thus, a towed bubble plume is more analogous to a bubble plume pulse in a horizontal current. Locally the two are identical; however, the boundary conditions are different. For a stationary bubble plume in a horizontal current (Fig. 1A), the bubble plume is surrounded by water with no vertical motion. In contrast, in a towed plume the "local" bubble pulse is bounded on the down-tow side by persistent upwelling flows driven by the pulse that already passed.

2. Materials and methods

2.1. Location

Two field tests were conducted from the *R/V Jan Mayen*, a 63.8-m, 4080-HP stern trawler to better understand the fluid dynamics of towed area bubble plumes. Towing tests were off the coast of Nordland (Andfjord) in northern Norway, 16–25 June 2008 (69°07.470′N, 16°00.836′E) with assistance by an auxiliary zodiac, and 22 April–05 May 2009, (69°08.006′N, 16°07.856′E) by the *R/V Hyas* (12.24 m 250 HP).

Wind, wave, and meteorological conditions were recorded periodically every few hours, or more frequently when significant changes occurred. Weather conditions on 20 June 2008 were highly favourable for the upwelling experiments; winds were calm and seas were flat. For the 25-m tow-tests on 22 June 2008, winds were up to 4 m s^{-1} and the significant swell was $H_s \sim 0.5$ m, primarily in the afternoon, while the following day for the 15 and 10-m tow tests winds reached ~6 m s^{-1} in the afternoon and swell was $H_s \sim 1.25$ m. Seagoing cruise conditions were ideal in 2009, with very low, upper-water turbidity, near calm winds (~2 m s^{-1}), and minimal swell (generally <20 cm).

2.2. Towed bubble rafts

Key system components are a submerged, towed air bubbler area diffuser, termed *bubble raft*, an air delivery system, and a collector net or surface skimmer. Two bubble raft orientations were deployed, one with the sparger elements parallel to the tow direction, termed *tow-parallel bubble raft*, and one with the sparger elements perpendicular or transverse to the tow direction, termed *tow-transverse bubble raft*. The tow-parallel bubble raft sought to maximize attachment flotation, while the tow-transverse bubble raft was designed for using upwelling flotation. A second difference was the bubble size distribution produced; the tow-parallel bubble raft produced far smaller bubbles than the tow-transverse bubble raft. Both were designed for tow depths from 10 to 30 m at tow speeds of 0.5–1.2 m s^{-1}.

2.2.1. Raft with tow-parallel sparging elements (2008 test)

A 21-m^2 bubble raft was constructed to produce very small air bubbles in a large area plume for marine application. Air was introduced into a seawater stream using a porous cylindrical sparging element placed inside a 50-mm diameter, 0.8-m long stainless steel

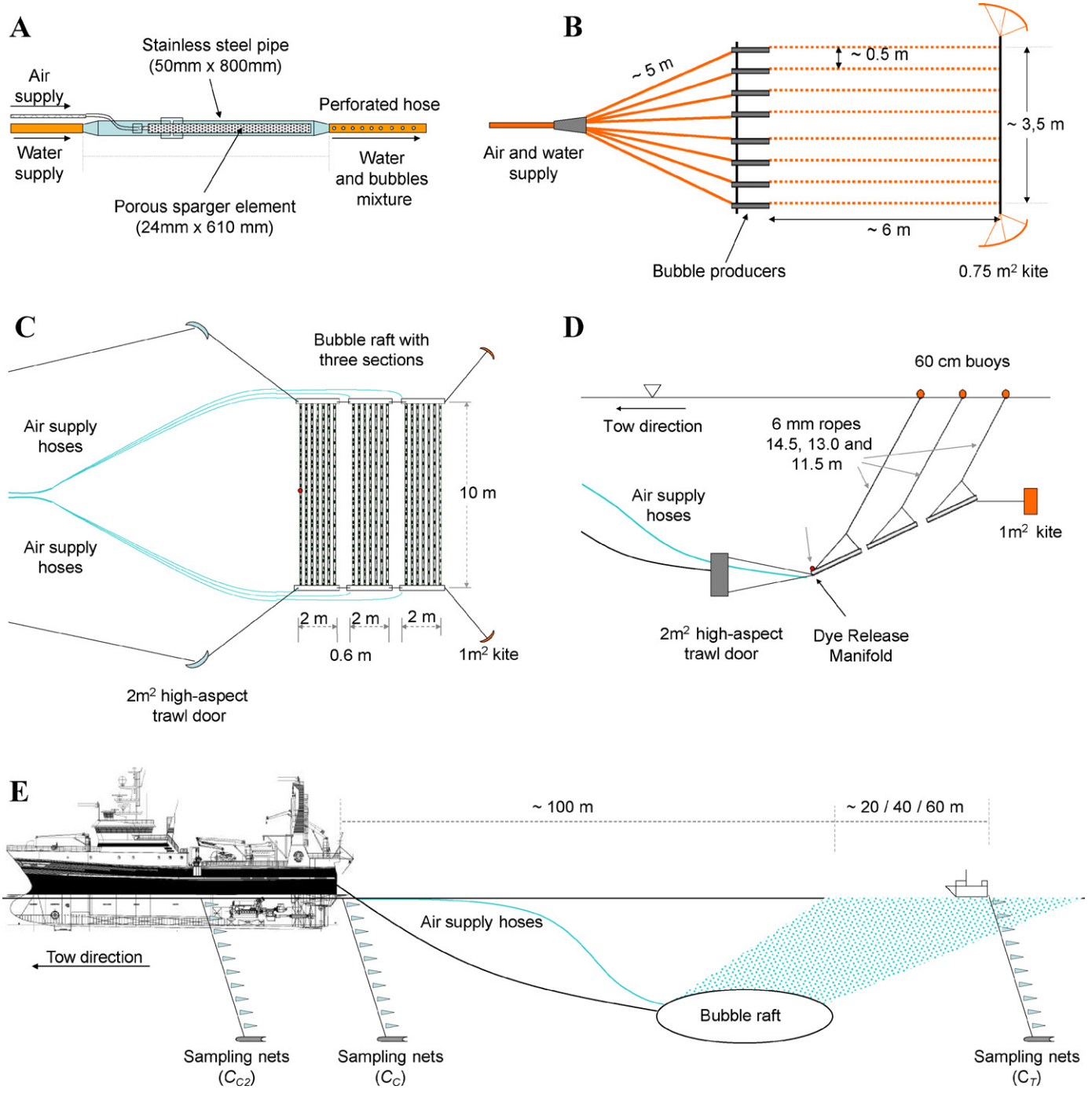

Fig. 2. Schematics for the bubble rafts: (A) Single bubble sparger element. (B) Top view of the raft with tow-parallel sparging elements. (C) Top view of raft with tow-transverse sparging elements comprised of 3 sub-raft elements and (D) side view. (E) Bubble raft and plankton net deployment.

pipe, which produced a large number of bubbles ~0.5–1 mm diameter that were mixed with the seawater flow inside the pipe (Fig. 2A). Each sparging element was an in-tank and/or Intrusive Sparger Element, 24-mm outer diameter, 610-mm long, and a Media Grate 2 (Mott Corporation, USA). Eight bubble sparger elements were fixed in parallel with 50-cm separation and attached to a 24-mm (1/2-inch) inner diameter, 6-m rubber hose with a large number of 6-mm holes drilled into it. Three holes were drilled every 10 cm along the hose at approximately equi-angular spacing. Two 3.5-m long aluminium tubes were affixed perpendicular to the sparging elements at the 6-m long raft's front and stern to provide rigidity.

The entire bubble raft was stretched and stabilized during towing by two 0.75-m^2 kites attached to the raft stern (Fig. 2B). Also, four 60-cm buoys were connected by 6-mm polyethylene ropes to the raft corners and helped maintain the bubble raft at the desired towing depth and provided visual location markers.

Air was supplied to the bubble raft through eight 12-mm (1/2-inch) inner diameter, 60-m air lines from a regulator manifold on the towing vessel. The manifold controlled each individual line through eight filter pressure regulators (NORGREN, Olympian Plus B64G) and included flowmeters (FL-2095, Omega Engineering, CT) to monitor the airflow. The flow rate and pressure were recorded for each line before and after each experiment, and generally were sta-

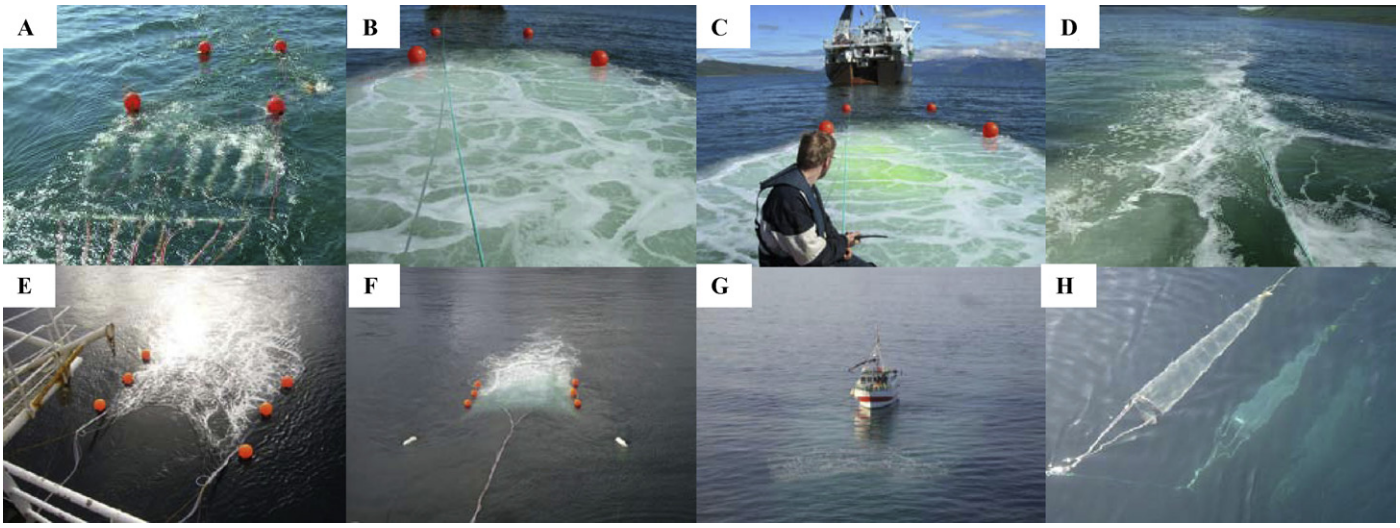

Fig. 3. Photos of the raft with tow-parallel sparging elements: (A) During deployment 20 June 2008, (B) Surface expression of the bubble plume for 4800 L min^{-1} air from 5-m depth. (C) Dye arriving at sea surface. Buoys are 60-cm diameter. *R/V Jan Mayen* stern is 120 m distant. (D) Surface bubble plume for 25 m deployment. Photos of raft with tow-transverse sparging elements: (E) During deployment on 29 April 2009. (F) The trawl doors spreading the bubble raft laterally. (G) *R/V Hyas* in position in bubble plume for sampling. (H) Tow sampling nets, note high visibility.

ble to better than the flowmeter precision. High pressure air supply to the regulator manifold was from a portable compressor (Mobilair M64, Kaeser, Inc., Germany) with an air delivery capacity of 6.4 m^3 dried air at 7-bar pressure and a regulated temperature of 7 °C. A maximum airflow to the raft of ~7200 L min^{-1}, at STP-standard temperature and pressure, was used during *Calanus* profile measurements.

Seawater was supplied from the towing vessel's seawater pump system to the bubble sparger elements by a mainline, ~100-mm (4-inch) inner diameter, 60-m rubber hose, which split into eight 24-mm (1-inch) inner diameter, 5-m rubber hoses (Fig. 2B). The seawater flow rate and pressure were controlled on board and recorded before and after each test. Two water flows were tested, 1000 and 1400 L min^{-1}; with the latter providing better distribution of the bubble–water mixture over the entire bubble raft. Thus, a water flow of 1400 L min^{-1} was used.

2.2.2. Raft with tow-transverse sparging elements (2009 test)

A second, 75 m^2 bubble raft was designed to generate a more homogeneous area bubble plume of larger bubbles and used transverse sparger elements (Fig. 2C). Bubble sparger elements were porous rubber soaker hoses, 12-mm inner diameter, which were assembled into three identical 25 m^2 raft sections, each with seven 10-m long spargers fixed in parallel and 33 cm apart and held in place by thin nylon strings. Spargers were connected on both ends to a 63-mm rigid PVC pipe, to which high pressure air was supplied from the towing vessel by six 60-m long, 19-mm (3/4-inch) diameter air supply hoses. The PVC pipes provided some structural stiffness as well as distributing the air from the air supply line to both ends of the 7-sparger elements, through two air supply lines for each raft section. The three raft sections were rigged to maintain an ~35° inclination angle while under tow. This angle was chosen to match typical bubble rise velocities in the bubble plume for a tow speed of 0.5 m s^{-1}. Thus, the raft continuously injects bubbles into the rising bubble sheet. The raft was designed with significant flexibility between sections to facilitate deployment/recovery.

Raft configuration (Fig. 2D) was maintained during towing by two 1 m^2 kites attached to rear corners of the raft, two, 2 m^2 high-aspect-ratio trawl doors attached to the front corners, and a series of 6-mm polyethylene ropes of different lengths attached to 60-cm buoys. Each bubble raft section was separated by 0.6 m. The raft was towed at a constant 15 ± 0.25 m depth, which was monitored with a pressure sensor (Model MP4-D, Scanmar AS, Norway).

The airflow of each supply hose was filtered, controlled, and measured by a regulator manifold similar to that described in Section 2.1. Flow rate and pressure were recorded for each supply line before and after each experiment, and generally were stable within measurement resolution. Flows up to 8432 L min^{-1} (STP) were produced with this setup and used during *Calanus* profile measurements.

2.3. Upwelling measurements

Upwelling flow, V_{up}, measurements were made for the parallel-sparger raft in 20 June 2008 off the coast of Andøya, Norway (69°02.470′N, 16°06.836′E) in water with depths between 216 and 307 m by injecting dye and measuring the transit time, t, for the dye to reach the sea surface. Values of t were determined with a stopwatch based on the first arrival time at the sea surface, when the boil exhibited green colour (Fig. 3C); and generally showed a high degree of repeatability. Measurements were made for a range of airflows, Q (2100–7200 L min^{-1} at STP), and release depths, z_0 (2.5, 5.0, and 7.5 m). Each combination had between 3 and 20 repetitions, depending on variability (more repetitions for higher variability data sets). For the transverse sparger bubble raft, the upwelling flow was measured for z_0 = 15 m and Q = 8432 L min^{-1} (STP). However, dye surfacing was difficult to observe and V_{up} was measured only for this combination.

Dye was injected from a manifold mounted at a central location on both rafts. The manifold was supplied with concentrated fluorescein dye solution through a 60-m long, 6-mm inner diameter hose. Air, water, and dye supply lines were bundled for better handling, to minimize flow disturbances, and to reduce hydrodynamic resistance during towing.

2.4. Calanus vertical profile measurements

The effect of the bubble-driven upwelling upon the *Calanus* vertical distribution was studied by comparing vertical profiles of *Calanus* catch samples before and after a given area had been trawled with the bubble raft. Standard plankton net arrays (20-cm diameter, 0.5-mm mesh opening) were towed for 30 min periods at sample depths, z_T (Fig. 3H). In 2008, z_T was 0.1, 1.0, 4.0, 7.0,

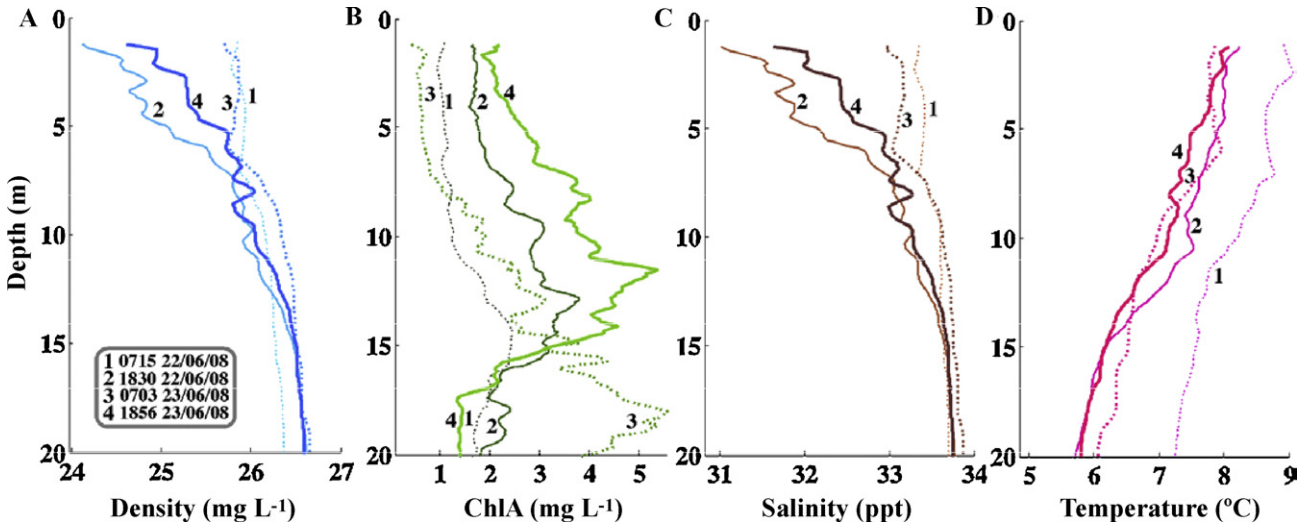

Fig. 4. Depth profiles on 22 June (1 and 2) and 23 June (3 and 4) 2008 for (A) density, (B) chlorophyll A, (C) salinity, and (D) temperature. Profile times labelled on panel A, dashed lines for morning profiles.

10.0, 13.0, and 16.0 m; in 2009, z_T was 0.1, 0.5, 2.0, 3.5, 5.0, 6.5, 9.5, 12.5, 15.5, and 18.5 m. For a 0.5 m s^{-1} tow speed, a sample net sweeps 28.3 m^3 of water. Test samples were collected from the zodiac whose position was maintained by a rope to *R/V Jan Mayen*, 25 m behind the initial upwelling boil and ~125 m behind *R/V Jan Mayen* (Fig. 3B and C). The sampling protocol followed involved first deploying the control nets, and then the test nets 60 s after the last control net entered the water. Retrieval followed the same order. This allowed the test and control nets to sample approximately the same water. Zodiac-collected samples were transported to the *Jan Mayen* for analysis followed by zodiac redeployment. In 2009, samples were collected 20, 40, and 60 m beyond the bubble plume's first surfacing location and analyzed onboard *R/V Hyas* (Fig. 3G). Reference (control) *Calanus* vertical profiles, $C_C(z_T)$, were measured from *R/V Jan Mayen*, while test vertical profiles, $C_T(z_T)$, were measured from the zodiac in 2008 and from *R/V Hyas* in 2009. The biovolume of *Calanus* was analyzed from the sample net catch by first excluding jellyfish, then emptying the sample into 50-ml graduated tubes, decanting water, and finally reading the *Calanus* volume.

In 2009, towing the bubble raft was attempted to one side of the *Jan Mayen's* wake to avoid hull flow and propeller wake effects on the vertical *Calanus* distribution. However, these attempts failed due to insufficient available warp length (max 40 m) to achieve the necessary sideways deflection. The *Jan Mayen*'s effect on $C_C(z_T)$ was characterized by comparison with a second control sampling net array, $C_{C2}(z_T)$, deployed on the *Jan Mayen*'s port.

2.5. Bycatch analysis

In 2008, catch samples also were analysed for bycatch. Samples to 10-ml volume (if available in the nets) were examined under a microscope and species other than *Calanus* were enumerated. Bycatch was divided into the following groups: *Brachyura indet* (true crabs), *Anomura indet* (hermit-, porcelain-, king crabs and squat lobsters), *Euphausiacea indet* (krill), shrimp (mostly juvenile stages), fish larvae, and fish eggs.

2.6. CTD vertical profile

To identify water-column stratification and to monitor water-column changes, profiles of temperature (T), salinity (S), and fluorescence were measured by CTD (SBE 25, Seabird Electronics, Inc.) casts. The CTD was equipped with a fluorometer (Seapoint Sensors, Inc.) to measure chlorophyll *A*.

3. Results

3.1. Oceanographic conditions before the tests

In June 2008, the raft with tow-parallel sparging elements was tested in the presence of strong upper water-column stratification. Temperature varied minimally with time except on 22 June 2008, when the water column cooled by ~1 °C (largely uniformly with depth and thus not affecting stratification). Stratification changes in the upper 5–7 m showed a tidal variation, with saline and well-mixed in the morning changing to fresher and more uniformly stratified water in the afternoon on both days (Fig. 4A and C). Chlorophyll *A* concentrations increased towards an asymmetric depth peak whose location exhibited a tidal trend, varying from 15-m at 07:15 LT on 22 June, to 13 m in the afternoon, then back down to 17 m the following morning (07:02 LT on 23 June), becoming shallower again later in the day (Fig. 4B).

In contrast, on 29 April 2009 when the raft with tow transverse sparging elements was tested, the water column was well mixed in the upper 20 m. On 30 April, the upper water column appeared stratified with a pycnocline between 10 and 15 m (Fig. 5A and C). Chlorophyll *A* values ranged between 1 and 6 mg L^{-1} with peak values observed between 10 and 20 m (Fig. 5B and D)

3.2. Bubble plume upwelling velocity

Plume upwelling velocities, V_{up}, were measured for the raft with tow-parallel sparging elements on 20 June 2008. V_{up} values were highly variable, but were mainly dependent on the air flow (Q). V_{up} ranged between ~10 and 25 cm s^{-1} and could be described by a power law fit, $V_{up} = Q^b$, where b varied between 0.246 and 0.323, depending on release depth (z_0) (Fig. 6). V_{up} for $z_0 > 7.5$ m was unsuccessful at advecting dye to the sea surface. For the raft with tow-transverse sparging elements, V_{up} was measured for the maximum airflow rate ($Q = 8432$ L min^{-1}) only and was 17.3 ± 2.4 cm s^{-1} for $z_0 = 15$ m.

3.3. Effect of bubble-driven upwelling on the vertical distribution of Calanus

Before testing the raft with tow-parallel sparging elements, on 22 June 2008, the *Calanus* distribution increased exponentially with depth ($C_C = 1.26e^{z/5.7}$, $R^2 = 0.992$) with the largest concentrations apparently deeper than 16 m and with few *Calanus* near the sea sur-

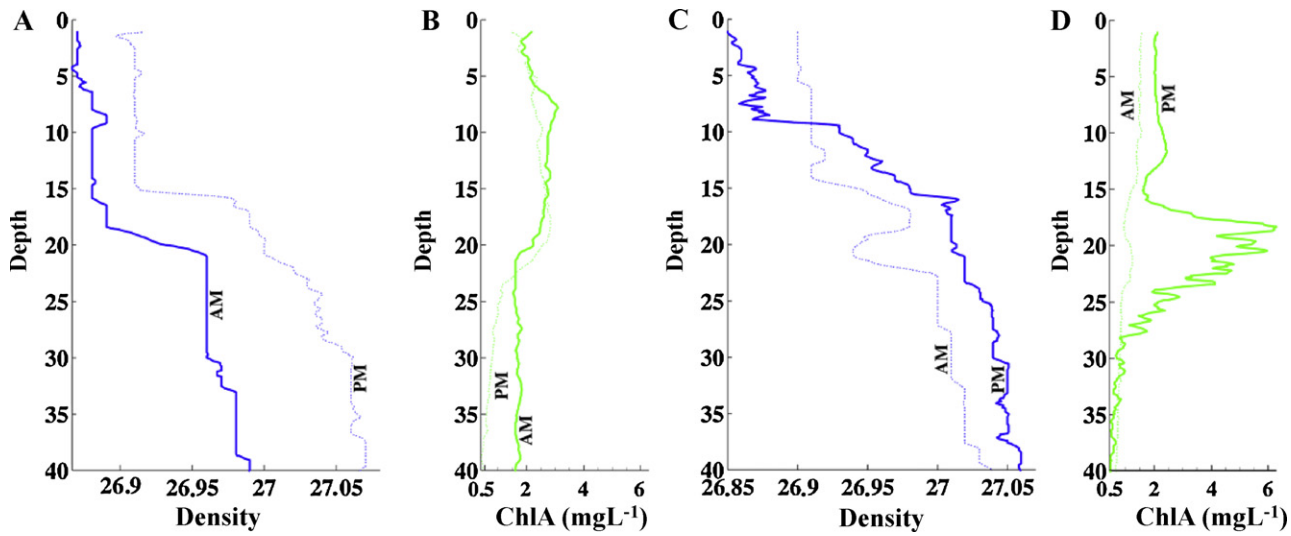

Fig. 5. Depth profiles on 29 April 2009 of (A) density and (B) chlorophyll A, and on 30 April 2009 of (C) density and (D) chlorophyll A.

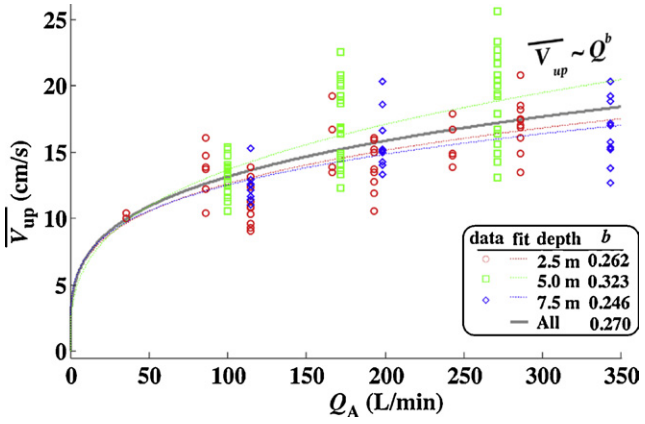

Fig. 6. Upwelling velocity (V_{up}) versus total airflow discharge, Q, for the release depths of 2.5, 5, and 7.5 m, and power law fits.

face. The bubble raft was towed at 25 m and had a significant effect on the *Calanus* profile, with near sea surface *Calanus* concentrations being only slightly lower than at 16 m. As a result, the exponential increase of $C_T(z)$ with z was far slower with $C_T = 8.02e^{(z/41)}$, $R^2 = 0.863$ (Fig. 7A). On 23 June 2008, the raft was towed at 15 m in the morning and at 10 m in the afternoon. The background *Calanus* profile, C_C, was reasonably well-described ($R^2 = 0.77$) by a double Gaussian layer, with peaks at 6 and 20 m (extrapolated), and by single broad (8.8 m) Gaussian centered at 7.2 m, respectively, with very few *Calanus* in the upper meter (Fig. 7A). After the bubble trawl, the *Calanus* distribution was shifted dramatically to shallower depths (Fig. 7B). The enhancement, defined by $\varepsilon = C_T/C_C$, showed similar trends for the three tow depths (Fig. 7C). For the 25-m tow, C_T increased as an exponential with a large half-depth from 15 m to the sea surface, indicating that significant upwelled *Calanus* were detrained from the rising bubble plume throughout the study depths ($z < 16$ m). Values for $\varepsilon(z)$ for the 15-m tow were decreased (<1) at depths of $12 < z < 4$ m, and showed the lowest surface value for the three tow depths. The 10-m tow showed the highest surface ε and the broadest increase with depth, i.e., the least concentrated, with its lowest values of ε for $6 < z_T < 10$ m. These depths likely

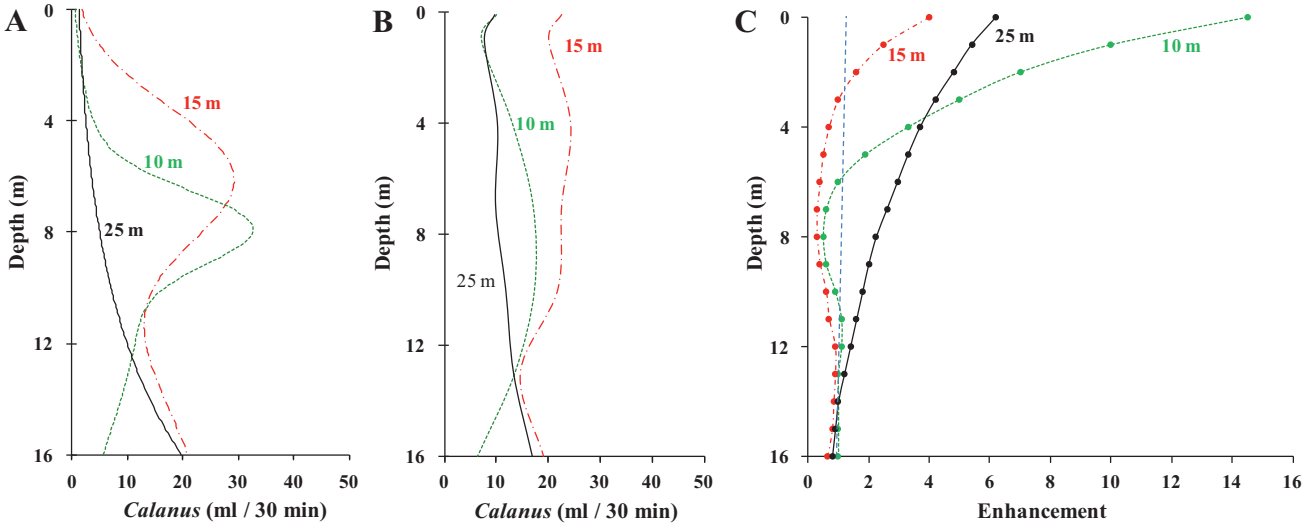

Fig. 7. Curve fits to *Calanus* sampling data for 22–23 June 2008, at tow depths of 25, 15, and 10 m. Data not shown for clarity. (A) Control plankton nets (C_C), (B) test plankton nets (C_T) and (C) enhancement (ε) based on curve fits (line) and data (symbols). Dashed vertical line indicates $\varepsilon = 1$.

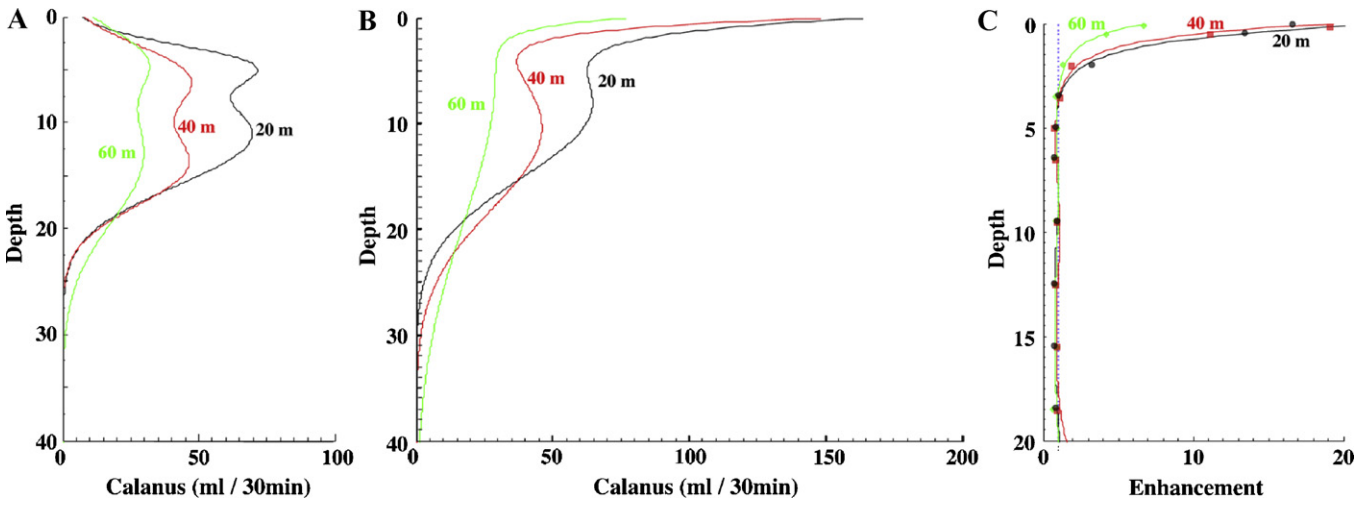

Fig. 8. Curve fits to *Calanus* sampling data for 29–30 April 2009, at 20, 40, and 60 m behind first bubble surfacing location. Data not shown for clarity. (A) Control plankton nets (C_C), (B) test plankton nets (C_T) and (C) enhancement (ε) based on curve fits (line) and data (symbols).

correspond to the initial acceleration phase, where *Calanus* were entrained into the bubble plume, making $\varepsilon < 1$.

Before testing the raft with tow-transverse sparging elements, on 29–30 April 2009, *Calanus* was distributed primarily in a layer from 4 to 16 m before the tow (Fig. 8A). After the tow, the bubble plume altered the profile significantly, concentrating *Calanus* in the upper 6 m (Fig. 8B). The largest *Calanus* concentrations were observed at 0.1 m depth. The difference between the control (C_{Cm}) and test (C_T) vertical profiles of *Calanus* was highly significant for all three sampling distances (Univariate ANOVA, $P < 0.001$) *Calanus* abundance was between ~30 and ~130% higher in the test nets compared to the control nets. The enhancement, ε, was highly significant. Specifically, had a 2-m tall *Calanus* net been placed at a depth of 1 m the catch enhancements, $_{z=0}\int^{z=2} \varepsilon\, dz$, would have been 980%, 770%, and 330% compared to a net placed elsewhere in the water column for 20, 40, and 60 m, respectively (Fig. 8C). Also, the larger enhancement is deeper than the surface layer, suggesting that the much of the *Calanus* enhancement arose from the sides. If the enhancement was from *Calanus* deeper than the surface layer, then the lower concentrations found at deeper depths should have been "advected" to shallower depths, causing a reduction ($\varepsilon < 1$).

3.4. Effect of propeller wake on the vertical Calanus distribution

The propeller and hull's effect on the vertical *Calanus* distribution was assessed during the two field studies by towing the bubble raft without producing bubbles. The *Test* plankton nets were towed 20 m behind the bubble plume's first surfacing location. No significant difference for the total *Calanus* concentration between C_C, C_{C2}, and C_T was found (Univariate ANOVA, $P > 0.786$). However, shallow *Test* samples caught significantly more *Calanus* than the *Control* nets (Fig. 9), while there was a slight reduction for $4 < z < 10$ m, suggesting some vertical mixing of the upper water column by the hull and/or propeller.

3.5. Effect of bubble-driven upwelling on the vertical distribution of bycatch

The level of bycatch and its taxonomic composition varied greatly, ranging from none (pure *Calanus*) to ~400 individuals per ml of sample. The most common bycatch was crabs (*Brachyura indet*, *Anomura indet*) at different larval stages. Fish eggs and larvae were present in some samples at levels up to 160 and 8 per

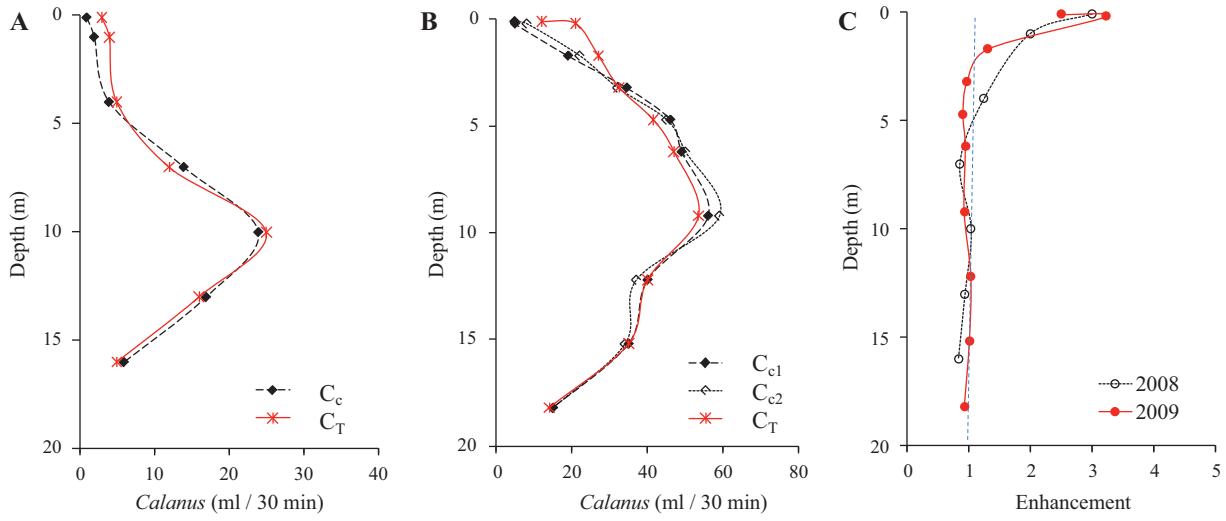

Fig. 9. *Calanus* catches of the *Test* (C_T) and the *Control* (C_C) sampling nets, which were collected when towing the bubble raft without producing any bubble plume on (A) 23 June 2008 and (B) 30 April 2009. (C) *Calanus* enhancement (ε) depth profiles from data curve fits for 2008 and 2009. Also shown is the *no enhancement* line ($\varepsilon = 1$).

Table 1
Mean bycatch reduction rates ($\varepsilon < 1$) at different tow depths, June 2008.

Bycatch	25-m tow depth	15-m tow depth	10-m tow depth	All
Brachyura indet	77.6	26.9	40.8	48.4
Anomura indet	84.6	60.0	84.3	76.3
Fish larvae	70.3	96.4	12.0*	51.6
Fish eggs	98.2	93.7	91.9	94.6
Euphausiacea indet	22.2	95.2	95.3	70.9
Shrimp	75.5	52.7	62.2	63.5

ml sample, respectively. However, the value for eggs was very uncertain because it was derived from very small sample volumes (0.1 ml). Mean vertical bycatch profiles showed significant reductions ($\varepsilon < 1$) for all organisms, except for fish larvae when the raft was towed at 10 m depth. Reduction rates varied between 48 and 95 (Table 1).

Bubble plume jellyfish flotation was effective, particularly by the plume's largest bubbles, which reached the sea surface prior to surfacing of the main bubble plume; although upwelling from the main plume also lifted jellyfish. These observations were highly encouraging, but bubble-plume jellyfish flotation was not quantified.

4. Discussion

4.1. Bubble upwelling and surface layer Calanus enhancement

The bubble trawl was highly successful at elevating *Calanus* concentrations in a thin surface layer. Surface enhancements, ε, as high as 1416% were observed in 2009. Although greater ε in surface layers were observed in 2008 in the presence of stratification, enhancement relative to the maximum in the water column, C_C, were far greater for the unstratified conditions of 2009 than 2008. In 2009, a *Calanus* trawl located at 20 m behind the bubble plume and fishing the upper meter would have in average increased the catch by 980%. These enhancements are dramatically larger than from hull mixing, which could not elevate *Calanus* concentrations greater than elsewhere in the water column.

Bubble raft design played a role. In 2008, the bubble raft created a bubble plume dominated by small bubbles, emphasizing attachment flotation. Further, these plumes were homogeneous at the sea surface, exhibiting convergence regions and presumably downwelling zones within the plume surfacing footprint. In 2009, the bubble raft was designed to create a strengthening, homogeneous bubble pulse, with the bubble sheet rise matching the bubble raft tilt leading to Q increasing with time. Visual observations suggest that large-scale, persistent near-surface eddies played an important role, by trapping bubbles (observed) and presumably *Calanus* (hypothesized). Certainly, the exponential *Calanus* profile in the upper few meters bears little resemblance to water-column characteristics (Fig. 5) or control *Calanus* profiles that were double Gaussian. Fortuitously, stratification was negligible to at least 15 m (tow depth) for most of the 2009 study. However, the bubble plume for the first meter or so above the bubble raft is in the acceleration phase, so the most significant fluid entrainment occurs somewhat shallower than the tow depth, the necking depth (Fanneløp and Webber, 2003). Thus, entrainment flows at the bubble source likely were driven by a significantly smaller V_{up} implying that deeper (denser) water entrainment was negligible.

Fluid motions originated by the towed bubble plume (Fig. 10) appeared to be more complex than for those originating from a stationary source, presumably due to the transient nature of towed bubble plume, the resultant bubble size segregation, and the interaction between persistent fluid motions and the rising bubbles (whose size distribution shifts towards smaller bubbles and thus lower total Q with time). Note, down-tow distance is equivalent to

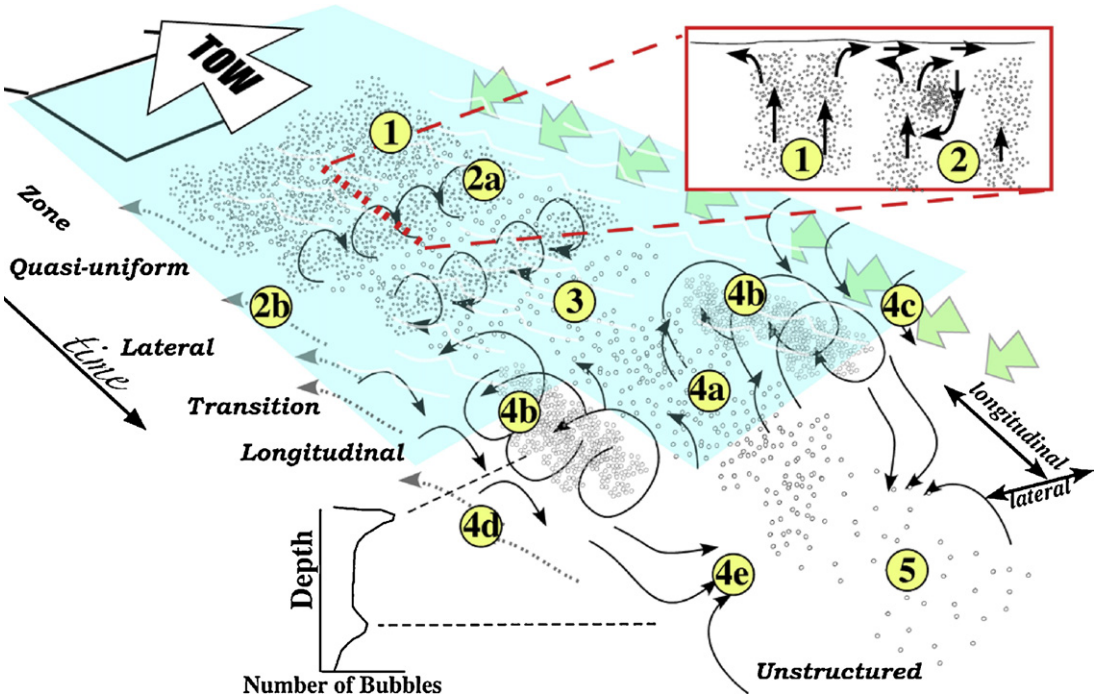

Fig. 10. Summary schematic of observed fluid motions and bubble spatial distribution for the transverse-element bubble raft. See text for description.

time; thus, Zone 1 becomes Zone 5 after a few minutes for a patch of water.

Where the bubble plume first surfaced (*Quasi-uniform Zone* (1)), bubbles showed no consistent spatial organization, rising in small and unsteady boils, as well as randomly in between. Bubbles here primarily were large. However, with increasing down-tow distance (time), bubble size generally decreased, as smaller, slower rising bubbles surface and the upwelling flow slows. Outwelling flows (horizontal surface intrusions) spread in all directions, including in the tow direction. The bubble plume is surrounded laterally by a momentum plume (dashed arrows, *Zones* 2–4). Thus, by continuity, inwelling (entrainment) flows are likely at some depth, and were visible further down tow (*Zone* 4). In the *Lateral Zone* (2), bubbles were organized into alternating linear vortices with bubbles trapped in their centre, separated by downwelling and upwelling zones. A proposed mechanism for this vortex formation is from the interaction between the outwelling flow when the upwelling flow is strongest, and the upwelling flow driven by bubbles later in the rising pulse (Fig. 10, inset). Needless to say, bubbles in the strongest upwelling flow surface first. Thus, with increasing down-tow distance (later in time), the upwelling and hence outwelling flow becomes weaker. As a result, the outwelling from the initial pulse in the downcurrent direction is stronger than the up-tow direction outwelling, and over-rides it. This could lead to vortex formation from the transformation of vertical upwelling momentum into angular momentum. In fact, toroidal structures are seen for stationary point-source bubble plumes where fluid from the downwelling flow outside the upwards momentum flow is re-entrained in the main upwelling flow (Lemckert and Imberger, 1993). Here, the tow geometry lends to linear rather than toroidal vortices.

Breakup of the lateral vortices is rapid, possibly due to instabilities, allowing trapped bubbles to escape in the *Transition Zone* (3). Shortly thereafter, two persistent (i.e., long), longitudinal vortices form in the *Longitudinal Zone* (4). The longitudinal vortices (4b) trap bubbles causing enhanced bubble densities (rendering the vortices highly visible) for tens of seconds or longer, and surround a central upwelling (4a) region where small bubbles and fluid rise. Outside the vortices are two longitudinally-oriented *Downwelling Zones* (4c), where bubbles are not observed rising, causing a sharp edge (tens of centimeters) to the location of the bubble plume. These downwelling zones are driven primarily by upwelled fluid, but also by slow inwelling fluid, which is observed as sea surface foam concentration. The momentum plume (4d) is expected to broaden and weaken with time, and must surface outside the longitudinal vortices. There also likely is asymmetry in the momentum plume with respect to current. However, details of the momentum plume were not measured in the field studies. Finally, in the *Unstructured Zone* (5), small bubbles rise to the sea surface, leading to a "wake" appearance, although associated flow motions were not observed.

Because the enhancement, ε, for depths shallower than ~4 m was significantly above 1, but there was no significant reduction ($\varepsilon < 1$) for deeper depths, increased *Calanus* in the water column must have been primarily from lateral bubble plume entrainment of *Calanus*. Some of the lateral entrainment could have arisen from deeper water ($z > 4$ m), compensating in part for the reduction in $C_T(z)$ due to vertical advection (upwelling) of a *Calanus* profile $C_C(z)$ that decreased with depth below 10–12 m. However, enhancements of 560–980% relative to the water-column maximum are difficult to explain by deeper entrainment and upwelling as they would almost certainly have caused a significant deviation from $\varepsilon = 1$ for $z > 4$ m. Given the absence of *Calanus* in the surface layer (C_C), lateral enhancement likely included an upwards component. Also, momentum plume upwelling, which surrounds the bubble plume, could have played a role through lateral *Calanus* entrainment.

4.2. Stratification and Calanus bubble trawl

Because a bubble plume does work lifting fluid against a density gradient, stratification can be a dominant factor in *Calanus* bubble trawl performance. Although 2009 ambient conditions fortuitously were largely unstratified in the upper 15 m (density variation <0.15 g L^{-1} for upper 20 m) (Fig. 5A) conditions in 2008 were significantly stratified (Fig. 4A). Unsurprisingly, there was a strong relationship between stratification and *Calanus* enhancement ($\varepsilon > 1$) and reduction ($\varepsilon < 1$).

At the sea surface, the rising upwelling flow becomes the outwelling flow. Where the rising fluid is denser (due to stratification), the outwelling flow has a sinking component. This sinking component depends on the density difference between the plume fluid and the ambient, which depends on the stratification and the plume strength. Specifically, the buoyancy flux of a *weak* bubble plume is less able to support denser fluid in a lighter ambient, leading to a greater number of detrainment intrusions during ascent (Aseda and Imberger, 1993).

In 2008, the outwelling flow was weak, the upper ocean was highly stratified, and unsteady convergence zones (patches of foam) were observed within the plume surfacing region (Zone 1). By continuity, these convergence zones must be associated with downwelling flows, which would transport *Calanus* away from the surface layer. In general, plume-induced downwelling has not been studied. However, it should be similar to single phase continuum flows in a downwards direction, albeit in the vicinity of the complex fluid motions associated with the bubble plume. The intrusion depth of the downwelled fluid should relate to stratification as well: fluid mixing during rise in the bubble plume means the equilibrium density is less than that of the water at its original entrainment depth (List, 1982). Thus, the exponential character of the *Calanus* profile after trawling (Fig. 8B) must arise from a combination of upwelling, outwelling, downwelling, and intrusion processes. The effect of stratification on raft performance may though be confounded by differences in raft design.

Investigation of the shift to positive enhancement (depth where *Calanus* detrainment + entrainment is positive) with respect to the density difference, ρ', gave values of 0.3–0.6 g L^{-1}, suggesting a limit for this plume to lift water against stratification. For 25 and 10-m tows, ρ' was 0.4 and 0.3 g L^{-1}, respectively, suggesting that tow depth was not a dominant factor. Other factors, such as plume dimensions or, more specifically, whether the bubble source is an area or point likely is important too. An area source at sufficient depth acts like a point source. This depth effect was observed for the raft with tow-parallel sparging elements (from the 25 m) where the surfacing bubble plume exhibited boils rather than the largely heterogeneous surfacing flow created by the raft with tow-transverse sparging elements (from 15 m). Further, high airflow bubble plumes transport water more readily against stratification, thus, Q likely plays a role in scaling. In these experiments, Q was the same for all bubble plumes (compressor maximum), except for dissolution reduction of Q for the 25-m tow. Clearly, more than three data sets are needed to properly characterize the effect of stratification on area plumes.

4.3. Bubble plume generation

Two highly distinct approaches were used to generate bubble plumes during the two field test series, one used a flushed sparger, that tended to produce very small bubbles (which a video camera mounted on the raft imaged as milky in appearence). The second used a porous rubber hose that produced larger bubbles (~1–2 mm diameter). Size distributions were not measured in the field (i.e., at depth, and under tow, and pressure) and significant deviations from laboratory bubbles are likely. With regards

to bubble processes, the smaller flushed sparger bubbles are less efficient at creating upwelling flows (Patro et al., 2002), but more efficient at attachment (own data, unpublished) than the larger bubbles from the porous rubber hose. Significantly, bubbles from the flushed sparger from 25-m depth did not always reach the surface, strongly suggesting that the bubbles produced were dissolving during rise. Bubble dissolution reduces the buoyancy flux, decreasing the plume's ability to transport fluid against stratification and maintain coherency against current and wave disruption.

The sparger element separation appeared to be too large, particularly at lower flow rates (upwelling study), where the plumes did not merge into a single plume. Specifically, the goal was to avoid having convergence zones and downwelling flows interior to the area bubble plume, because such flows represent a (potentially significant) loss of Calanus. From 25 m, stronger sea surface boils (relative to the outwelling velocities) were observed than for shallower depths. These boils represents a loss of coherence of the plume-driven fluid motions, and thus should decrease upwelling, while also creating strong downwelling flows, and playing a role in lower ε for 2008 than 2009.

A key advantage of the porous rubber hose sparger elements, aside from producing larger bubbles, is that resistance to air flow through the hose pores creates a significant internal overpressure relative to hydrostatic. As a result, small hydrostatic pressure changes from waves, and variations in tow depth and sparger element tilt, etc., have minimal effect on the bubble emission rate along the hose, yielding relatively uniform, steady-state bubble emissions. In contrast, bubbles from a non-porous, drilled rubber tube were highly sensitive to hydrostatic pressure, such that portions of the hose under wave crests produced less to no bubbles.

4.4. A continuous injection bubble pulse

The raft with tow-transverse sparging elements produced a truly novel bubble plume, continuously injecting bubbles into the same volume. Where a bubble pulse is produced from a stationary area plume and Q increases as the bubble plume rises due to decreasing hydrostatic pressure, the increase in buoyancy flux is non-linear, and except for near the sea surface, small. For example, for a 20-m plume with $V_{up} = 20\ cm\ s^{-1}$, Q doubles after bubbles have risen for 50 s. In comparison, the towed bubble raft's Q for the first meter doubles after 1 s during which the plume has only risen ~0.5 m, with additional increases in Q from hydrostatic expansion. On the other hand, because the bubble plume locally is a pulse, fluid acceleration is continuous. The upwelling flow generated was far less for the raft with tow-parallel sparging elements than for the raft with tow-transverse sparging elements due largely to the pulse-like nature of the bubble plume. Currently, bubble pulse behaviour, particularly for an area plume, remains completely uncharacterized, while this is the first reported continuous-injection bubble pulse.

4.5. Synergistic upwelling and flotation

Although the focus of the raft with tow-parallel sparging elements was attachment flotation and that of the raft with tow-transverse sparging elements was upwelling flotation, both processes occurred for both rafts. Moreover, the two processes are synergistic, *Calanus* with attached bubbles likely have greater difficulty escaping from the bubble plume, including when trapped in a turbulence vortex, and the added buoyancy increases their upwards velocity. Further, for *Calanus* to escape the bubble trawl, they need to jump away from the bubbles, which likely is less efficient for individuals with attached bubbles.

One interesting and potentially important feature of vortex trapping is that it places zooplankton and bubbles in close proximity with numerous opportunities for bubble-zooplankton interaction and aggregation formation. Thus, significant *Calanus* could have some bubble attachment, aiding the upwelling process. Also, upwelled zooplankton likely become trapped in vortices, and the upwelling flow prevents downward escape. Lateral escape for zooplankton, even at the plume edge, likely is inefficient because of the inflow and the jump response is random when confronted by bubbles (own data, unpublished). Further, some fraction of *Calanus* that do escape may be re-entrained in the upwelling flow in the bubble plume.

4.6. Bubble trawl bycatch reduction

The upwelling flow and the vortices appeared to be effective at trapping other copepod-sized species, although healthy fingerlings were not caught, suggesting that they were not upwelled of lifted by bubble attachment. The towed bubble plume reduced by 65% of all types of bycatch organisms, which were in the path of the bubble plume. The greatest reduction was for crabs (in different larvae stages) and fish eggs, which initially were concentrated in a shallow layer (<3 m) and likely were floated towards the sea surface by the bubble plume. At the surface, the effect of the outwelling flow apparently removed them laterally, making them unavailable for the sampling nets. Because sampling was not performed at the bubble plume edges, the fate of these bycatch organisms is unclear. The bubble plume's effect upon fish larvae and especially upon small fish seems different from that for crab larvae and fish eggs. Accordingly, while the bubble attachment processes may have enhanced the flotation of crabs and fish eggs (presumably because of hair and stickiness of fish eggs); bubble attachment to fish larvae and fingerlings seems highly improbable. Also, visual evidence of small fish swimming inside the bubble plume suggests that fish larvae and fingerlings may have actively avoided the bubble plume.

The largest (~3–4 mm diameter) bubbles surfaced first and apparently were highly effective for jellyfish flotation. This not only represents a great advantage for bubble-enhanced *Calanus* harvesting, but also for conventional fine-meshed trawls for *Calanus* and other fisheries. For example, jellyfish flotation could divert jellyfish from the trawl path, avoiding associated problems with net clogging, catch damage, sorting, etc. Jellyfish flotation appears distinct from *Calanus* flotation, in that due to the morphology of the jellyfish, bubbles readily are trapped in their body, leading to more effective buoyant rise. For example, jellyfish were very common in 2008 and were observed floating at the sea surface with entrapped bubbles. Although the bubble trawls were not designed to effectively divert jellyfish through flotation; such diverters could be very useful for improving the *Calanus* fishery.

5. Conclusions

The area bubble plume-enhanced *Calanus* harvesting technology, presented in this paper, is a unique and novel design that improved copepod catch rates, reduced bycatch, and significantly decreased energy consumption during towing by allowing for a smaller collector. Results showed very strong *Calanus* enhancement relative to elsewhere in the water column in a thin surface layer during tests in the absence of stratification. Stratification was a dominant factor affecting bubble trawl performance; however, data were insufficient to characterize stratification's effect on bubble plume fluid motions beyond fluid-ambient density difference.

Investigation of the bubble generation approach suggested small bubbles are problematic, particularly for deeper tow depths where dissolution becomes significant, compared to larger bubbles. Large bubble generation was effective by pressurizing a porous rubber hose – the pressure difference across the hose walls prevented

hydrostatic pressure changes (swell) from causing emission variability along the sparger elements, in contrast to a drilled rubber hose. The current bubble trawl design, while appropriate for these field tests, lacked robustness for commercial application. Although highly promising, results highlighted significant areas of critical need for further study: increased sampling resolution, validation of the vortex *Calanus* trapping hypothesis, and characterization of the role of stratification in bubble plume processes related to bubble trawl performance.

Acknowledgments

We thank Jon Terje Eilertsen for help with the instruments on board Jan Mayen; and Snorre Angell, Ivan Tatone, Trond Larsen and Lasse Rindahl for their valuable assistance on field work. Thanks to the crews of the Hyas and Jan Mayen. This work was funded by the Research Council of Norway through the Oceans and Coastal Areas Program (HAVKYST), project 178421/S40, "Harvesting zooplankton by bubble flotation".

References

Aksnes, D.L., Blindheim, J., 1996. Circulation patterns in the North Atlantic and possible impact on population dynamics of *Calanus finmarchicus*. Ophelia 44, 7–28.
Aseda, T., Imberger, J.T., 1993. Structure of bubble plumes in linearly stratified environments. J. Fluid Mech. 249, 35–57.
Dahle, T., Kaartvedt, S., 2000. Diel patterns in stage-specific vertical migration of *Calanus finmarchicus* in habitats with midnight sun. ICES J. Mar. Sci. 57, 1800–1818.
Falkenhaug, T., Timonin, T., Tande, K., 1997. Abundance and distribution of numerical important species of zooplankton in summer and winter periods of 1990 and 1991 in North Norwegian fjords. J. Plankton Res. 19 (4), 449–468.
Fanneløp, T.K., Webber, D.M., 2003. On buoyant plumes rising from area sources in a calm environment. J. Fluid Mech. 497, 319–334.
Johnson, B.D., Cooke, R.C., 1980. Organic particle and aggregate formation resulting from the dissolution of bubbles in seawater. Limnol. Oceanogr. 25 (4), 653–661.
Kattner, G., Krause, M., 1987. Changes in lipids during the development of *Calanus finmarchicus* s.l. from Copepodid I to adult. Mar. Biol. 96, 511–518.
Lalli, C.M., Parsons, T.R., 1997. Biological Oceanography. The Open University.
Leifer, I., Boles, J., 2005. Measurement of marine hydrocarbon seep flow through fractured rock and unconsolidated sediment. Mar. Petrol. Geol. 22 (4), 551–568.
Leifer, I., Jeuthe, H., Gjøsund, S.H., Johansen, V., 2009. Engineered and natural marine seep, bubble driven buoyancy flows. J. Phys. Oceanogr. 39 (12), 3071–3090.
Leifer, I., Clark, J.F., Chen, R.F., 2000. Modifications to the local environment by natural marine hydrocarbon seeps. Geophys. Res. Lett. 27, 3711–3714.
Leifer, I., Luyendyk, B., Boles, J., Clark, J.F., 2006. Natural marine seepage blowout: contribution to atmospheric methane. Global Biogeochem. Cycl., 20, doi:10.1029/2005GB002668, GB3008.
Leifer, I., Patro, R.K., 2002. The bubble mechanism for methane transport from the shallow sea bed to the surface: a review and sensitivity study. Cont. Shelf Res. 22 (16), 2409–2428.
Leifer, I., Judd, A., 2002. Oceanic methane layers: a bubble deposition mechanism from marinehydrocarbon seepage. Terra Nova 16, 471–485.
Lemckert, C.J., Imberger, J., 1993. Energetic bubble plumes in arbitrary stratification. J. Hydraul. Eng. 119, 680–703.
List, E.J., 1982. Turbulent jets and plumes. Ann. Rev. Fluid Mech. 14, 189–212.
Mao, L., Yoon, R.-H., 1997. Prediction flotation rates using a rate equation derived from first principles. Int. J. Miner. Proc. 51, 171–181.
Mari, X., 1999. Carbon content and C:N ratio of transparent exopolymeric particles (TEP) produced by bubble exudates of diatoms. Mar. Ecol. Prog. Ser. 183, 59–71.
McDougall, T.J., 1978. Bubble plumes in stratified environments. J. Fluid Mech. 85, 655–672.
Milgram, J.H., 1983. Mean flow in round bubble plumes. J. Fluid Mech. 133, 345–376.
Mizukawaa, K., Takada, H., Takeuchi, I., Ikemoto, T., Omori, K., Tsuchiya, K., 2009. Bioconcentration and biomagnification of polybrominated diphenyl ethers (PBDEs) through lower-trophic-level coastal marine food web. Mar. Pollut. Bull. 58 (8), 1217–1224.
Nicol, S., Endo, Y., 1999. Krill fisheries: development, management and ecosystem implications. Aquat. Living Resour. 12 (2), 105–120.
Patro, R.K., Leifer, I., Bowyer, P., 2002. Better bubble process modelling: improved bubble hydrodynamics parameterization. In: Donelan, M. (Ed.), Gas Transfer at Water Surfaces. American Geophysical Union, Washington, pp. 315–320.
Persechini, M.A.M., Jota, F.G., Peres, A.E.C., 2000. Dynamic model of a flotation column. Miner. Eng. 13, 1465–1481.
Singleton, V.L., Gantzer, P., Little, J.C., 2007. Linear bubble plume model for hypolimnetic oxygenation: full-scale validation and sensitivity analysis. Water Resour. Res., 43.
Schadlow, G., 1992. Bubble plume dynamics in a stratified medium and the implications for water quality amelioration in lakes. Water Resour. Res. 28 (2), 313–321.
Solomon, E.A., Kastner, M., MacDonald, I.R., Leifer, I., 2009. Considerable methane fluxes to the atmosphere from hydrocarbon seeps in the Gulf of Mexico. Nat. Geosci. 2, 561–565.
Skjoldal, H.R., Dalpadado, P., Dommasnes, A., 2004. Food webs and trophic interactions. In: Skjoldal, H.R. (Ed.), The Norwegian Sea ecosystem. Tapir Academic, Trondheim, Norway, pp. 447–506.
Skjoldal, H.R., 2005. The Norwegian Sea Ecosystem. Tapir Academic Press.
Tande, K.S., Miller, C.B., 2000. Population dynamics of *Calanus* in the North Atlantic: results from the trans-Atlantic study of *Calanus finmarchicus*. ICES J. Mar. Sci. 57 (6), 1527–11527.
Topham, D.R., 1975. Hydrodynamics of an oil well blowout. Beaufort Sea Tech. Rep., Ocean Sci., Sidney BC, No. 33.
Unstad, K., Tande, K., 1991. Depth distribution of *Calanus finmarchicus* and *C. glacialis* in relation to environmental conditions in the Barents Sea. Polar Res. 10 (2), 409–420.
Wu, J., 1995. Mechanisms of animal cell damage associated with gas bubbles and cell protection by medium additives. J. Biotech. 43, 81–94.